JGR Space Physics

RESEARCH ARTICLE
10.1029/2022JA030275

# Solar Flux Influence on the In-Situ Plasma Density at Topside Ionosphere Measured by Swarm Satellites

**Chao Xiong[1,2], Haicheng Jiang[1], Rui Yan[3], Hermann Lühr[4], Claudia Stolle[5], Fan Yin[1], Artem Smirnov[4,6], Mirko Piersanti[7], Yiwen Liu[8], Xin Wan[9], Piero Diego[7], Zeren Zhima[3], Xuhui Shen[3], Matthias Förster[4], Stephan Buchert[10], and Dieter Bilitza[11,12]**

[1]Department of Space Physics, Electronic Information School, Wuhan University, Wuhan, China, [2]Hubei Luojia Laboratory, Wuhan, China, [3]National Institute of Natural Hazards, the Ministry of Emergency Management of China, Beijing, China, [4]GFZ German Research Centre for Geosciences, Potsdam, Germany, [5]Leibniz Institute of Atmospheric Physics at the University of Rostock, Kühlungsborn, Germany, [6]Institute of Physics and Astronomy, University of Potsdam, Potsdam, Germany, [7]Department of Physical and Chemical Sciences, University of L'Aquila, L'Aquila, Italy, [8]School of Physics and Electronic Information, Shangrao Normal University, Shangrao, China, [9]Planetary Environmental and Astrobiological Research Laboratory (PEARL), School of Atmospheric Sciences, Sun Yat-sen University, Zhuhai, China, [10]Swedish Institute of Space Physics, Uppsala, Sweden, [11]Department of Physics and Astronomy, George Mason University, Fairfax, VA, USA, [12]Heliospheric Laboratory, NASA Goddard Space Flight Center, Greenbelt, MD, USA

**Key Points:**

- First comprehensive comparison of Ni measured by the Langmuir probe (LP) and faceplate (FP) on board Swarm satellites is performed
- There exists a systematic difference between the LP and FP derived Ni values, and it varies with solar flux, local time, and season
- LP-derived Ni shows a clear dependence on solar flux, caused by ion compositions change at Swarm altitude during low solar flux years

**Correspondence to:**
C. Xiong,
xiongchao@whu.edu.cn

**Citation:**
Xiong, C., Jiang, H., Yan, R., Lühr, H., Stolle, C., Yin, F., et al. (2022). Solar flux influence on the in-situ plasma density at topside ionosphere measured by Swarm satellites. *Journal of Geophysical Research: Space Physics*, *127*, e2022JA030275. https://doi.org/10.1029/2022JA030275

Received 8 JAN 2022
Accepted 12 APR 2022

**Abstract** In this study, we perform the first comprehensive comparison of ion density (Ni) in the topside ionosphere measured by the Langmuir probe (LP) and faceplate (FP) of the thermal ion imager on board Swarm satellites. Our results show a systematic difference between the LP and FP derived Ni values, and the systematic difference shows prominent dependences on solar flux, local time, and season. Although both Ni datasets show generally good linear regression with electron density (Ne) measurements from the incoherent scatter radar (ISR) located at Jicamarca, the Ni derived from LP shows an additional dependence on the solar flux, while such a dependence cannot be seen in the FP-derived Ni. We suggest that the solar flux dependence of LP-derived Ni is related to the ion compositions change at Swarm altitude, which has not been properly accounted for in the LP processing algorithm. More light ions (e.g., $H^+$), diffusing down from the plasmasphere to the Swarm altitude, seem to cause the overestimation of Ni from LP during low solar activity. A linear relation between the Swarm LP-derived Ni and ISR Ne is derived, and such a function is recommended to be implemented into further updates of the Swarm LP plasma density data.

## 1. Introduction

Earth's ionosphere is the ionized part of the upper atmosphere, spanning roughly the range from 60 to 1,000 km altitude. Two important parameters for a description of the ionosphere are the plasma density and temperature; therefore, different techniques have been developed for precisely measuring the two parameters. Compared to remote sensing facilities from the ground, for example, ionosonde or incoherent scatter radar (ISR), in-situ measurements from satellites provide continuous and global coverage. As a result, low-earth orbiting (LEO) satellites have become an important data source for improving our understanding of the topside ionosphere (e.g., Benson et al., 1977; Brace, 1998; Sagawa et al., 2005; Wan et al., 2021). Among a series of spaceborne payloads, the Langmuir probe (LP) is a conventional instrument that has been frequently installed on satellites or rockets for probing the ionosphere, due to its simplicity, relatively small weight and low power consumption (Brace et al., 1971, 1998; Oyama, 2015).

The Langmuir probe (LP) includes an electrode immersed into the plasma, with either planar, cylindrical, or spherical shape. The basic theory of measuring plasma density and temperature using Langmuir probe (LPs) was developed by Langmuir and his colleagues (e.g., Mott-Smith & Langmuir, 1926). By applying a direct current voltage varying from negative to positive, the electrode attracts ions and electrons from the ambient plasma, leading to a measurable current. In the so-called ion saturation region, when the applied voltage has a sufficient negative bias relative to the surrounded plasma potential, the current is carried almost entirely by the positive ions. While in the electron saturation region with a sufficiently positive bias, current is resulting from the electrons. In the region between the ion and electron retardation region, the current varies exponentially with the bias of a scale factor proportional to the electron temperature, Te. Based on the analysis of current-voltage

(I-V) characteristics, the number density of ion/electron as well as Te can be estimated (e.g., Brace et al., 1971; Chapkunov et al., 1976; Lebreton et al., 2006). However, it is worth to note that there is not a universal theory of LPs applicable for all measurement conditions, because the analytic current-voltage (I-V) characteristics are derived under certain assumptions, for example, the orbital motion limited (OML) theory (Chen, 2009; Tonks & Langmuir, 1929), factors, like the probe size, geometry, material, and platform potential etc., will lead to additional uncertainties of the plasma density and temperature estimates (e.g., Resendiz Lira & Marchand, 2021).

Comparison from earlier satellites equipped with long-wire LPs found that the in-situ measured Te is generally higher than the values from ground-based radars (Brace, 1998). Hanson et al. (1969) compared the Explorer 32 overflights of incoherent scatter radar (ISR) at Jicamarca, and found the Te from LP was by about 70% higher. Similar overestimates have also been reported from the OGO-6 satellite, showing higher values of Te by about 15% (McClure et al., 1973). Later from a shorter LP on board the Atmospheric Explorer-C (AE-C) satellite, much better agreement was found between the in-situ Te and radar values (Benson et al., 1977). This result suggested that the accuracy of earlier long probe measurements may have suffered from the inaccurately inverted current-voltage (I-V) characteristics. One possible reason could be that the surface patchiness of long probes and geomagnetically induced potentials can cause energy smearing of the electron retardation regions at very low Te, and such influences have not been taken into account in the I-V curve inversion (Brace, 1998). For later satellite missions, like the Challenging Mini-satellite Payload (CHAMP) (Reigber et al., 2002), Gravity Recovery and Climate Experiment (GRACE) (Tapley et al., 2004), and China Seismo-Electromagnetic satellite (CSES) (Shen et al., 2018) etc., comprehensive comparisons have been made between the in situ electron density with ground-based measurements before the datasets being released (McNamara et al., 2007; Xiong et al., 2015; Yan et al., 2020). In addition, the LP measurements onboard an orbiting platform sometimes can also provide insights in differences between ground-based facilities. Benson et al. (1977) have compared the Te from the Atmospheric Explorer-C (AE-C) satellite with four radars located at different locations (Millstone Hill, Chatanika, St. Santin, and Arecibo). The only disagreement was found at Millstone Hill, which was lower than the LP measurements by an average of 11%. This result uncovered a systematic bias between the radar measurements from Millstone Hill and from facilities at other locations (Brace, 1998).

With an increased number of facilities over the globe and also the accumulated data sets during the past decades, measurements from ground radar and ionosonde have been extensively used for comparison and validation of in-situ measurements from recent satellite missions (e.g., Lei et al., 2007; Lomidze et al., 2018; McNamara et al., 2007; Rother et al., 2010; Xiong et al., 2015). Meanwhile, in-situ measurements from different missions can also be used for cross-validation (e.g., Pedatella et al., 2015; Smirnov et al., 2021; Wang et al., 2019; Yan et al., 2020). Such efforts can reveal and eliminate the possibly existing systematic discrepancies between different data sets, and they further help to improve ionospheric empirical modeling (e.g., Bilitza & Xiong, 2020).

European Space Agency (ESA's) on-going Swarm mission, consisting of three identical satellites, aims to precisely monitor the Earth's magnetic field and upper atmosphere (Friis-Christensen et al., 2008). Lomidze et al. (2018) performed a comprehensive validation campaign of Swarm LP measured Ne and Te, by comparing the data with observations from incoherent scatter radar (ISRs), ionosondes, and the Constellation Observing System for Meteorology, Ionosphere, and Climate (COSMIC) satellites estimates. Their results revealed a generally good agreement between Swarm and other data sets; though, the Swarm LP underestimated the Ne by about 21% compared to the ISR values. Recent studies also proved that the in-situ plasma densities measured by Swarm LP are excellent to survey ionospheric structures (e.g., Astafyeva et al., 2016; Buchert et al., 2015; Jin et al., 2020; Wan et al., 2018; Zhou et al., 2016). The special constellation of Swarm, for example, during the initial mission phase when the three satellites flew in a string-of-pearls formation, maked it possible to distinguish the temporal from spatial variations of small-scale field-aligned currents at high latitudes (Lühr et al., 2014) as well as of the ionospheric irregularities at equatorial and low-latitudes (Xiong, Stolle, et al., 2016); and of the east-west magnetic field gradient measured by the lower pair of satellites flying side-by-side, helping the lithospheric magnetic field modeling to achieve an unprecedented accuracy (Thébault et al., 2016).

In a recent effort, Bilitza and Xiong (2020) managed to improve the topside Ne estimation of the International Reference Ionosphere model during extremely low solar activity levels, by including measurements from several low-earth orbiting (LEO) satellites, such as, Alouette, International Satellites for Ionospheric Studies (ISIS), CHAMP, GRACE, and Swarm missions. Good agreement of regression parameters is deduced between the topside sounder of Alouette and International Satellites for Ionospheric Studies (ISIS) as well as in-situ Ne from

CHAMP and GRACE, but an additional scaling factor needs to be applied to the Swarm Ne, in order to obtain agreement of absolute values with the other data sets (see Figure 4 of Bilitza & Xiong, 2020). As mentioned above, the in situ Ne measurements from CHAMP (McNamara et al., 2007), GRACE (Xiong et al., 2015) and Swarm (Lomidze et al., 2018) showed quite well agreement with ground-based ISR observations. One possible reason could be that the Swarm Ne data used by Lomidze et al. (2018) were from December 2013 to June 2016, while Bilitza and Xiong (2020) used the Swarm Ne data from 2013 to 2020, covering the very low solar activity years 2018–2019. This suggests that uncertainties might exist in the Swarm Ne data during very low solar activity conditions. In addition to the 2 Hz plasma data from the onboard LP, the faceplate (FP) of the thermal ion imager (TII) occasionally provides plasma density with a higher sample rate of 16 Hz (Knudsen et al., 2017). To our knowledge, no extensive cross-validation between the plasma densities from the two instruments has been performed so far. So, a detailed comparison between two data sets has been pending, and such a comparison will be helpful for identify if the LP data of Swarm underestimate the Ne during low solar activity years.

The content of this study is arranged as follows: in Section 2, we first provide a short introduction of the LP and faceplate (FP) instruments, as well as recent updates of Swarm LP data processing. In Section 3, a detailed comparison between the two data sets is performed, by resolving the local time (LT), seasonal, and solar flux dependences. In Section 4, the LP and faceplate (FP) derived density data have been further compared with the ISR measurements at Jicamarca. In Section 5, possible reasons that may cause the discrepancy between the two data sets are discussed. Finally, our findings are summarized in Section 6.

## 2. Data Set and Approach

### 2.1. Swarm LP and FP

The Swarm LP and FP (embedding the TII) are part of the Electric Field Instrument (EFI) package, and a detailed description of EFI can be found in Knudsen et al. (2017). There are two LPs mounted on the earthward edge of the Swarm ram panel, and the two LPs are separated by 30 cm and located quite close to the faceplate of TII. The radius of both spherical probes is 4 mm and the distance from the center of the sphere to the platform is 99.01 mm (Resendiz Lira & Marchand, 2021). The surface material of one probe is Titanium Nitride, and the other probe surface is made of gold-plated Titanium to reduce the chemical reactivity with ionospheric Oxygen (Catapano et al., 2021).

Each of the three Swarm spacecraft is equipped with a FP, in which two TIIs are embedded. The FP is of rectangle shaped with an area of $351 \times 229$ mm$^2$, and its thickness is 3.175 mm (Resendiz Lira & Marchand, 2021). The primary objective of the TIIs is to measure the plasma drift, but when they are not in operation, the current collected by the FP and the shells of TIIs can be measured at a sample rate of 16 Hz, thus the FP can be used as a planar LP with a fixed-bias voltage (typically $-3.5$ V) to the spacecraft. The relation between collected ion current and density can be derived by considering the plasma flow being supersonic in the spacecraft reference frame and the FP operating in the ion saturation region. We want to emphasize that the FP provides Ni only when the TIIs are not active, namely for certain orbits per day (see later in our Figure 2).

### 2.2. Some Important Aspects of Swarm LP

Here we only repeat some important aspects of the Swarm LP, which might lead to the uncertainty of its plasma density estimations.

#### 2.2.1. Sweep Mode and High-Frequency Harmonic Mode

Two methods are conventionally used to measure currents collected by the probes as a function of voltage. One is the full sweep mode, in which the probe bias voltage is varied from a sufficiently negative potential (the ion saturation region) up to a sufficiently positive potential (the electron linear region). Another approach, referred as high-frequency harmonic mode, focuses on the parts of I-V characteristics needed to infer the density and temperature. In the harmonic mode, the probe voltages are modulated sinusoidally at a certain frequency and with a variable amplitude depending on the characteristic region. For Swarm, the harmonic technique runs at 128 Hz to measure the currents collected by the spherical probes. This is the first time that the harmonic mode is used in orbit to obtain the I-V characteristic of space plasma (Knudsen et al., 2017). The high frequency harmonic mode used most of the time, while the classical sweep mode occurs each 128 s, and lasts for 1 s. During the full

sweep mode, the I-V curve is traditionally measured but the data are not included in the Swarm Level-1B plasma processor. They are separately analyzed and provided as an additional advanced data product by ESA (Catapano et al., 2021).

#### 2.2.2. High Gain and Low Gain

Another important aspect of the Swarm LP is that each of the two LPs can be commanded to a high or low gain, in order to avoid an automatic gain control which would potentially interfere with reliable and accurate current measurements. The term "gain" should be understood here rather as a sensitivity of the current measurement than an amplification. The first analysis, preceding Baseline 04 of the Swarm Level-1B products, estimated the electron density and electron temperature from the high gain probe for low densities currents while from the low gain probe for high densities currents, and by blending the results from both probes for an intermediate range of density current. However, it was found out later that the regularly occurring transition between probes with different gain produced non-physical variations of the estimated parameters even when smoothed by the intermediate blending (Catapano et al., 2021). Therefore, the algorithm to estimate the density was changed to use the weaker ion current instead of the retarded and saturated electron currents. The ion current and admittance are always and very reliably measured by the high gain probe. The density product is therefore rather Ni, though often designated still as Ne in some publications. We want to point out that the Ne and Ni are assumed to be equal at ionospheric altitudes, due to the electric neutrality of plasma. This modification has been introduced with Baseline 05 at ESA's servers. As shown in Catapano et al. (2021), only slight differences have been found between the plasma densities of Baselines 04 and 05. In this study, we used the Ni product from Baseline 05. To exclude the outliers of Ni from LP, only data points with "Flags_LP = 1, Flags_Ne = 20, Flags_Versus = 20" have been considered. The detailed information about these flags can been found in Catapano et al. (2021).

### 2.3. Ne Measurements From the ISR at Jicamarca

Ne from the ISR located at Jicamarca has been used for further validating the Ni measurements from Swarm. Under oblique mode (antenna elevation of 87.06°), the Jicamarca ISR provides nearly vertical electron density profiles ranging from 100 km to above 1,000 km. The Ne data from the ISR are publicly accessible at the open Madrigal database (http://cedar.openmadrigal.org).

To find the conjunctions between ISR and Swarm, three criteria have been applied: (a) the difference in coordinated universal time (UTC) between Swarm and ISR measurements should be less than 15 min; (b) the longitudinal difference between two techniques should be less than 15°, which limits the LT difference within 1 hr; (c) for the corresponding altitude Ne profile from ISR, an exponential fit has been applied to the altitude range of ±75 km centered on the Swarm cruising altitude; if the standard deviations of the exponential fit with respect to the altitude profile exceeds a threshold of 40%, the profile is not used. The criterion (c) is intended to exclude the altitude profiles when the Ne distribution is quite dynamic. A similar approach has been used by Xiong et al. (2015) for validating the GRACE satellite measured Ne against ISRs at different latitudes.

The ISR data used for comparison are from December 2013 until the end of 2020, as no oblique mode data are available in 2021. After applying the above-mentioned criteria, it yields 162/51, 154/59, 175/81 conjunction events of the ISR at Jicamarca and with the LP/FP for the three Swarm satellites, A, B, C, respectively.

## 3. Comparison of the Ni Measured by the Swarm LP and FP

Figure 1a shows the magnetic latitude (MLAT) profile of Ni from one orbital segment of Swarm A at low and middle latitudes, when it crossed the equator at 22:47:56 UTC on 7 March 2015. The black and red curves represent the Ni values measured by the LP and FP, respectively. Intense equatorial plasma depletions (EPDs) are observed from both curves. Such EPDs, also called equatorial plasma bubbles, are often observed during post-sunset hours and have been addressed in details based on the Swarm observations (e.g., Rodríguez-Zuluaga & Stolle, 2019; Wan et al., 2018; Xiong, Stolle, et al., 2016). The latitudinal variations of the two curves agree well with each other, but with a 16 Hz sample rate the Ni from FP reflects much finer structures than the 2 Hz data from LP (Figure 1b). In addition, the absolute values of Ni from FP are larger than the values from LP, which indicates that there is a systematic difference between plasma densities measured by the two instruments.

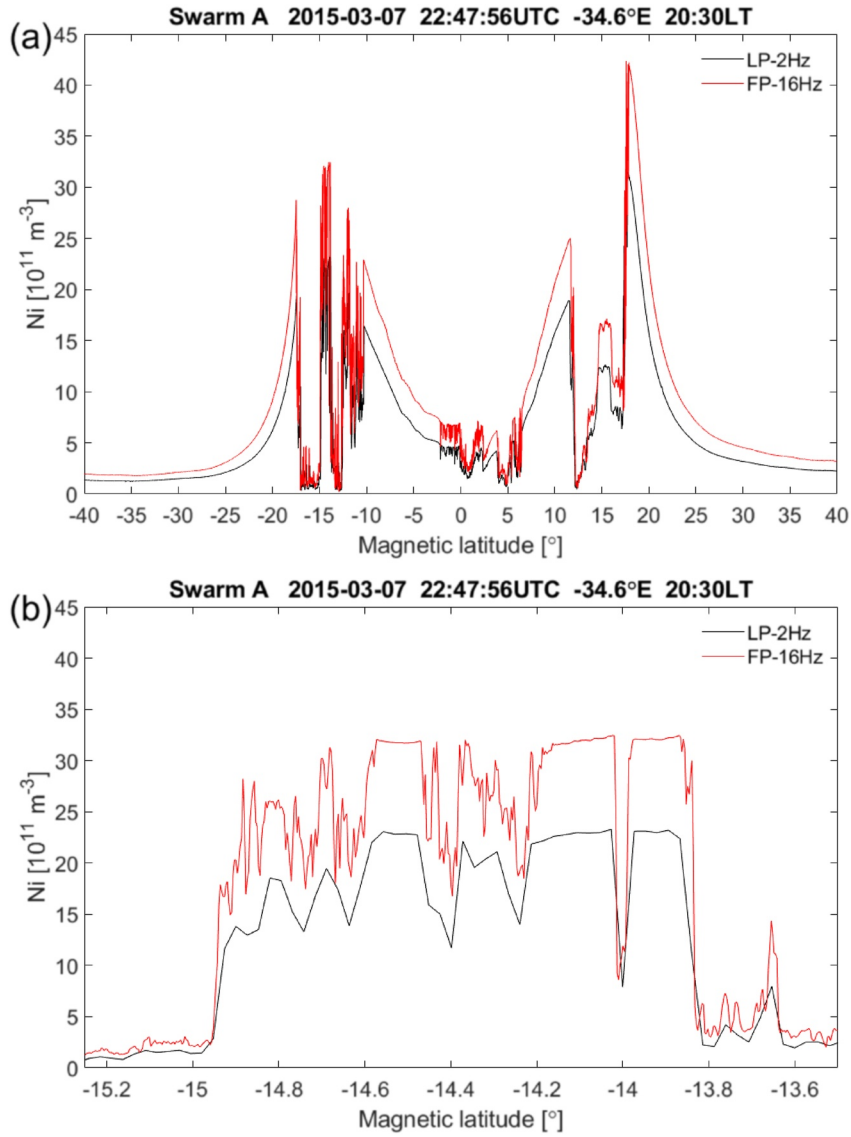


**Figure 1.** (a) The latitude profile of Ni from one orbital segment of Swarm A at low and middle magnetic latitudes (MLAT), when it crossed the equator at 22:47:56 UTC on 7 March 2015. Black and red curves represent the Ni measurements from the Swarm Langmuir probe (LP) and faceplate (FP), respectively. (b) A zoom-in profile of Ni between −15.25° and −13.5° MLAT.

As an overview, the top two panels of Figures 2a–2c show the solar flux index and altitude variations for the three Swarm satellites, respectively. The P10.7 is defined as P10.7 = (F10.7 + F10.7 A)/2, where F10.7 A is the average value of F10.7 over 81 days. As mentioned above, both solar flux indices slowly decrease from above 200 sfu at the end of 2014, to below 70 sfu in 2018–2019, and afterward they start to recover again since the end of 2019. During the initial mission phase, the three satellites flew at the same altitude (about 500 km); after the orbit maneuvers were completed, on 17 April 2014, Swarm A and C flew at about 470 km, while Swarm B was about 50 km higher. The orbits of the three satellites slowly decayed during the past 7 years, due to the neutral air drag. At the end of November 2021, Swarm A and C reached about 430 km and Swarm B about 500 km. For each satellite, the Ni data from LP and FP have been presented in the bottom two panels. They are sorted into MLAT bin of 2°, and averaged over each day. The LP is continuously operated from the beginning of the mission and provides data almost every day. The FP data are available since 2 October 2014 and is operated relatively sparsely since 7 October 2019 for Swarm A and B, and since 27 July 2020 for Swarm C. The blank areas in the third panel are due to a lack of FP data. The Ni data from both instruments exhibit similar temporal and latitudinal variations. At

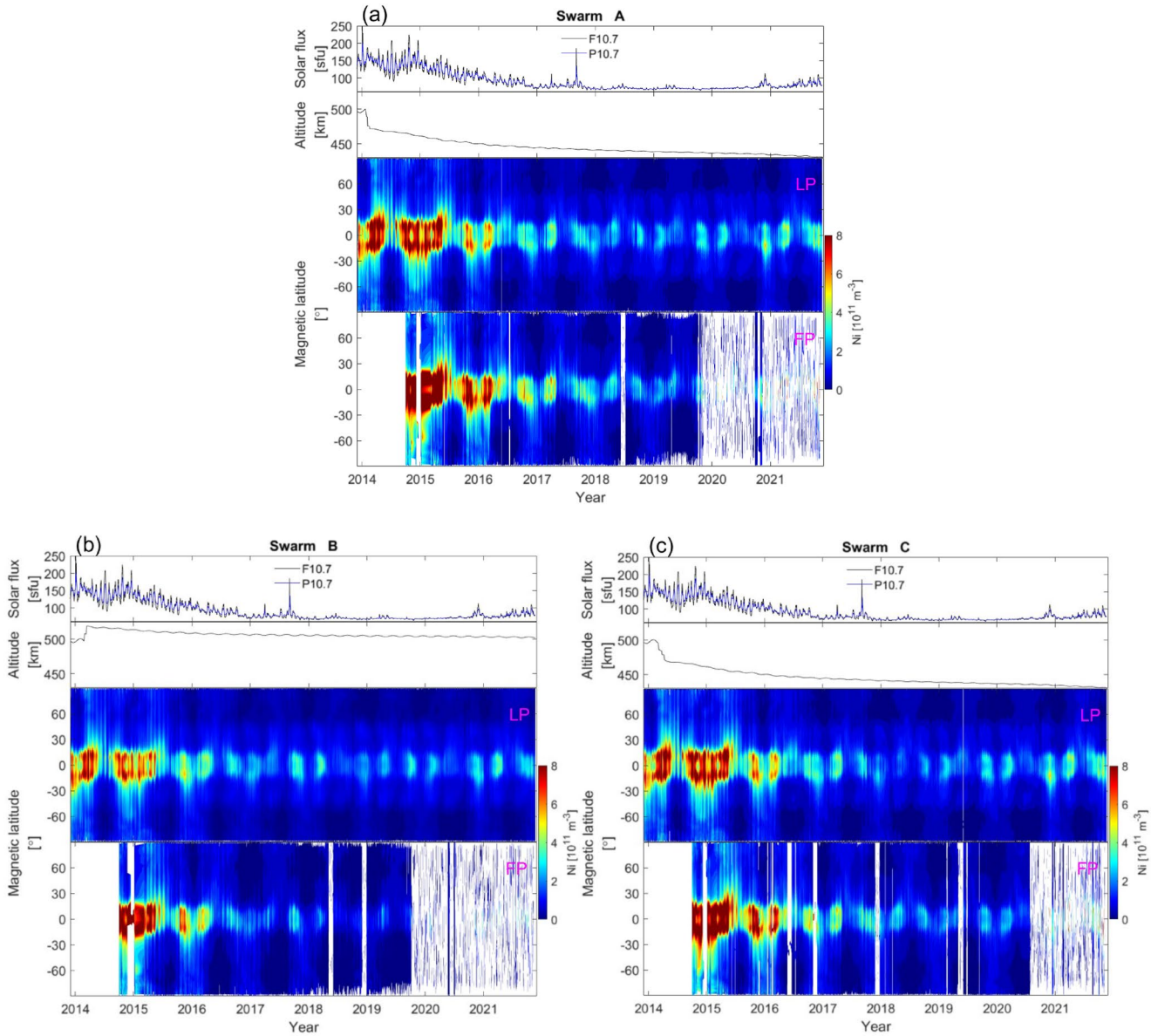


**Figure 2.** The solar flux and altitude variations over time are shown in the top two panels and the MLAT versus. date distribution of Ni derived from the LP and FP in the bottom two panels for the three Swarm satellites in frame (a–c), respectively.

the equatorial and low latitudes, the well-known equatorial ionization anomaly structure (e.g., Appleton, 1946) dominates, and its intensity shows a clear dependence on solar flux level, for example, Ni slowly decreases from 2014 to 2019 and then starts to increase again. In addition, a typical seasonal variation is also seen, with the largest values of Ni at the two equinoxes and lowest values around the June solstice. At higher latitude, the ionospheric middle latitude trough is prominent during local winter, namely around December solstice in the northern hemisphere and June solstice in the southern hemisphere. In addition, the intensity of the middle latitude trough is much deeper and lasts longer during low solar flux years. This feature seen by Swarm is consistent with earlier observations from the CHAMP and GRACE satellites (Xiong et al., 2013). Besides the agreement and similarity, we also note that the Ni absolute values measured by FP are larger than those from LP during 2014–2016 (e.g., with a relative difference of −19.2% for Swarm B), which reflects well with the example shown in Figure 1. However, the situation seems to be reversed during the low solar flux years, for example, 2017–2019, with larger Ni values from LP (especially for Swarm B, with a relative difference by about 24.3%). This result suggests that the systematic difference between Ni values measured by LP and FP changes with time.

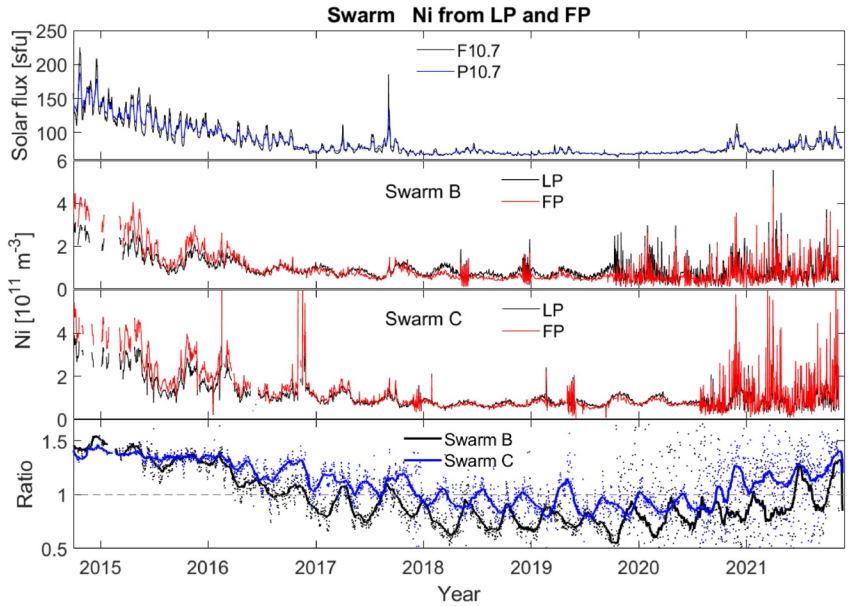


**Figure 3.** Variations of solar flux indices (top panel), daily averaged values of Ni from Swarm B (second panel) and from Swarm C (third panel); the ratios of Ni derived by faceplate (FP) over that from Langmuir probe (LP) for the two satellites (bottom panel).

To better assess the relative variation of Ni from LP and FP, we use the ratio between the two datasets, which is defined as Ni_FP/Ni_LP, and the result is shown in Figure 3. Note, as Swarm A and C fly side-by-side and their plasma density from LP are fairly consistent (e.g., Xiong, Zhou, et al., 2016), in the following we only show the result from Swarm C, as it has longer FP data coverage. The result from Swarm B is also shown, which represents the situation at a higher altitude. To better compare with the solar flux variation, the F10.7 and P10.7 curves have been repeated in the first panel of Figure 3. The daily averaged Ni values have been further averaged over all latitudes and they are separately presented in the second and third panels for Swarm B and C, with black and red curves representing results from LP and FP, respectively. It has to be noted here, although data are averaged over 24 hr, all readings of a day come practically from the same LT sectors, being separated by 12 hr for the ascending and descending arcs. The Swarm orbits precess only slowly through local times. The Ni curves follow each other quite well, showing prominent solar flux and seasonal variations. Noticeable differences between the two curves are seen, with larger/lower values from LP before/after 2017, respectively. During the deep solar minimum (2018–2019), the difference between the two curves is much more prominent for the higher-flying Swarm B.

Quite dynamic variations of Ni (with many spikes) are seen beginning in October 2019 and July 2020 for Swarm B and C, respectively. These dates correspond well to the time when the FP data coverage becomes sparse for the two satellites. For example, two periods of Ni oscillations of Swarm B are seen in 2018, and the two periods correspond well with the data gaps evident in the third panel of Figure 2b. We want to note that for making a fair comparison between LP and FP, for deriving the curves in Figure 3, we only considered the periods when Ni from both instruments (LP and FP) are available. For each orbit the 16 Hz Ni data from FP has been first down-sampled to 2 Hz, and then averaged in the same way as for the LP. The Ni spikes most likely reflect the longitudinal variation of the low-latitude ionosphere, which cannot be smoothed out because the FP data become sparse. Such spikes cannot be seen in the LP data, as shown in Figure 2, when we make use of all the continuous LP measurements, and as a result the longitudinal variations of the ionosphere are smoothed out in the daily averages.

From October 2014 to November 2021, the ratios (black and blue dots) for both satellites gradually decrease from 1.5 to below one and then increased again. After applying a sliding-average over a period of 27 days, the ratios show clear periodical variations with periods of 141 and 133 days for Swarm B and C, respectively. Such periods represent the number of days needed for the two Swarm satellites to cover all 24 hr of LT, which also suggests that the systematic difference between LP and FP depends on LT. The ratios attain peak values when data are collected from the 06 and 18 magnetic local time (MLT) sector. Minima are related to noon and midnight orbits.

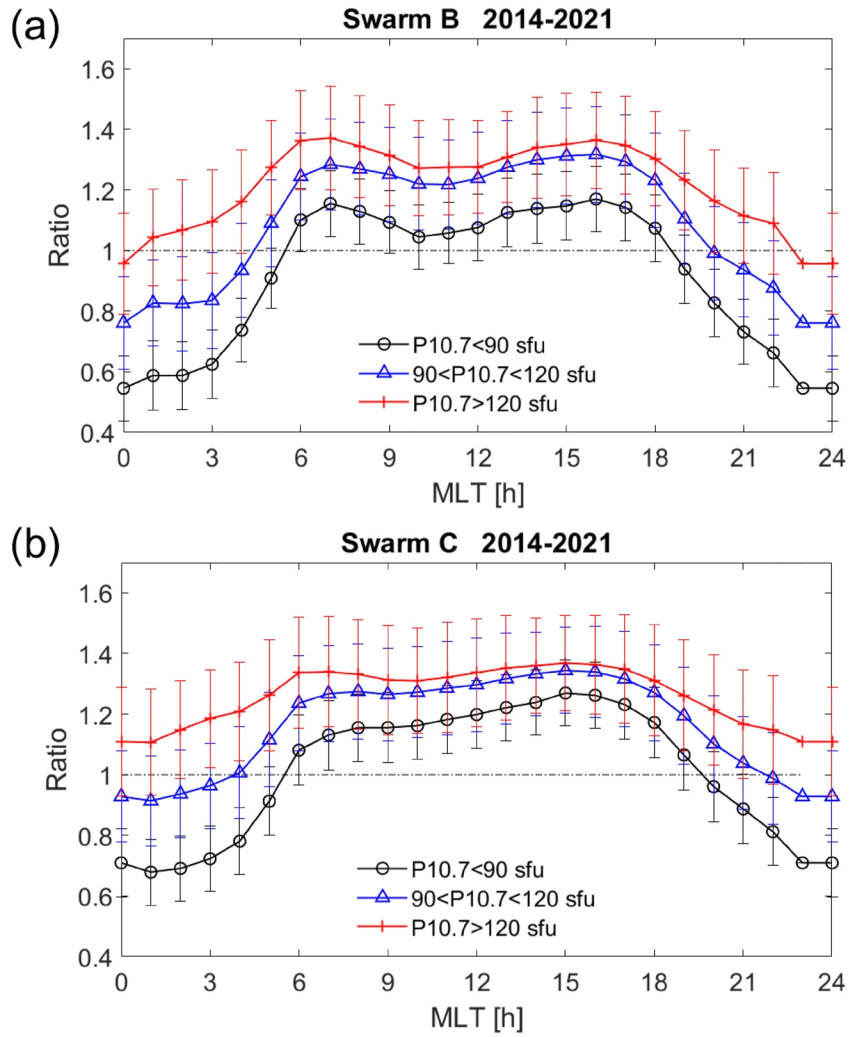


**Figure 4.** The MLT dependence of the ratios between faceplate and Langmuir probe derived Ni, separately for Swarm B (a) and Swarm C (b). For both satellites the data set have been divided into three different solar flux classes.

This suggests larger Ni overestimations of LP from noon plus midnight passes. Compared to Swarm C, the ratio of Swarm B goes to lower values at low solar flux years, suggesting also an altitude dependence of the systematic difference between LP and FP. Figure 4a further presents the dependence of the ratio of Swarm B on MLT. Data have been divided into low, moderate and high solar flux levels, indicated by the solar flux index ranges: P10.7 < 90 sfu, 90 ≤ P10.7 ≤ 120 sfu, and P10.7 > 120 sfu. Mean values within 1 hr MLT bins are presented as black circles, blue triangle, and red crosses for the three solar flux levels, respectively, and the standard deviations of the hourly mean values are also represented. Similar MLT dependences are found for the ratios at all three solar flux levels, that is, the ratios are smaller on the nightside than the values on the dayside. Under low solar flux condition, the reversal of ratio (larger/smaller than 1) appears at 06:00 and 19:00 MLT; while under moderate solar flux condition, the reversal has been shifted to 04:00 MLT on the morning side, and postponed to 21:00 MLT at nighttime. For high solar flux condition, relatively lower values are found at the nighttime, but the ratio stays above 1 for all MLT hours, implying the LP measured Ni are always larger than the values from FP. The ratios from Swarm C in Figure 4b show similar solar flux and LT dependences, but with systematically higher values than that of Swarm B (see Figure 4b). An interesting feature is that a valley of the ratio is found around 10:00–11:00 MLT for both Swarm satellites under all solar flux levels.

Figure 5a shows the seasonal variation of the ratios for Swarm B. The daily averaged ratios under the three solar flux levels are presented by smaller black circles, blue triangles, and red crosses, respectively, and the monthly

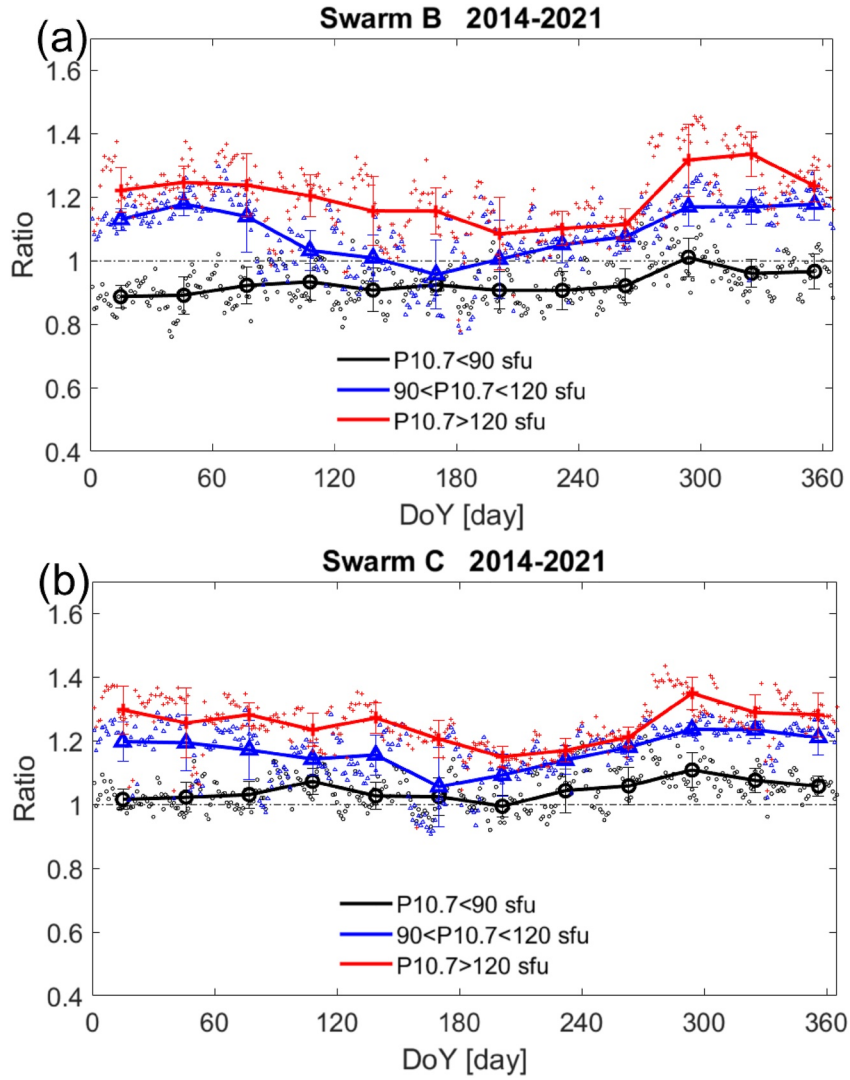


**Figure 5.** The same as Figure 4, but for the seasonal variations of the ratio.

mean values are presented with larger symbols. The standard deviations of the monthly mean values are also presented It is found again that the ratio is smaller for lower solar flux level. Slightly higher values are found at the beginning of March and end of October and lowest around June solstice for both moderate and high solar flux levels, while the ratios stay more or less constant throughout the year under low solar flux level. For Swarm C, as shown in Figure 5b, similar solar flux and seasonal dependences are observed, but the absolute values of the ratio are clearly larger.

## 4. Validation Against the ISR at Jicamarca

The previous section showed that the ratios between Ni values derived from the Swarm LP and FP instruments and their ratios exhibit dependences on solar flux, season, and local time. Besides the relative variations of Ni, the absolute values are also important, especially for empirical ionosphere modeling. Therefore, we further compared the Swarm plasma densities to the Ne measurements derived by the ISR at Jicamarca, because ISR is one of the most powerful ground-based facilities for providing reliable ionospheric parameters.

Figure 6a shows the linear regression between Ni from the LP of Swarm B and Ne from the ISR. Conjunctions from different years are marked with different colors. Although underestimating by about 26%, the Ni from LP agree quite well with the ISR Ne measurements, achieving a correlation coefficient of 0.90. However, when

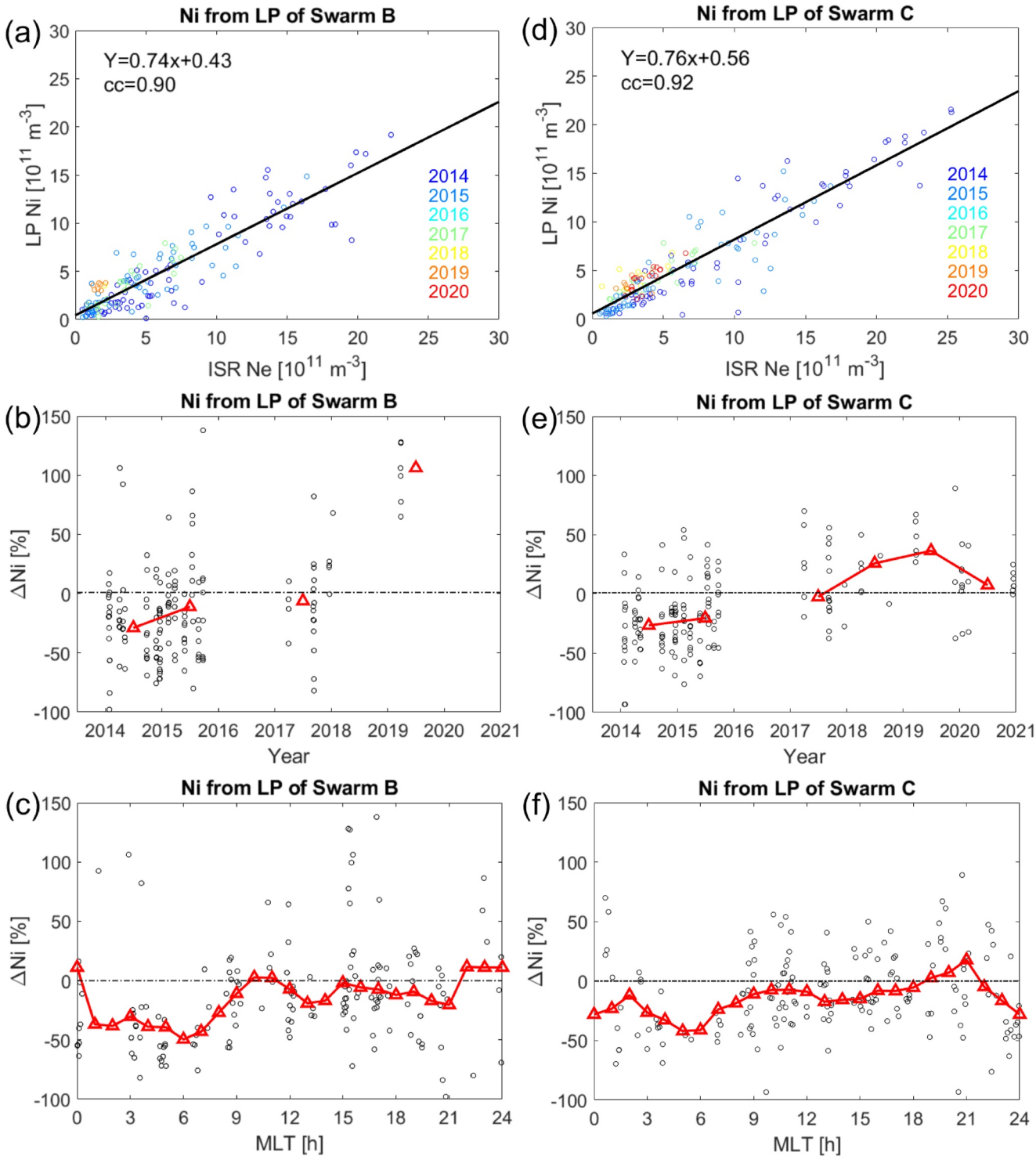


**Figure 6.** Linear regression between the LP derived Ni and ISR Ne (top), their relative differences over year (middle) and MLT (bottom). The results from Swarm B and C have been separately presented in the top and second bottom frames.

looking at the situations for different years, we find that the Ni from LP are larger than the ISR measurements at low solar activity years (red circles). Figure 6b shows the relative difference, defined as ΔNe = (Ni_LP-Ne_ISR)/Ne_ISR, and their annual median values are marked by red triangles. The relative difference slowly increases from about −25% in 2014 to about 100% in 2019, indicating that the LP of Swarm B underestimates the plasma

densities during 2014–2017, but overestimates the densities in 2019. From Figure 6c, we see that the Ni from LP better agreement on the dayside ($\Delta Ni < 25\%$), but show larger discrepancies on the night side ($\Delta Ni$ of about $-40\%$). This result is consistent with the conclusion from Catapano et al. (2021). The results from the LP of Swarm C are shown in Figures 6d–6f, which also reveal a nice linear dependence with the Ne from ISR. The correlation coefficient reaches 0.92 and an overall underestimation by about 24% is obtained. The relative difference shows much clearer variations over the years, which increases from about $-25\%$ in 2014 to about 50% in 2019 and then decrease again back to zero in 2020. The variation of the relative difference agrees well with the solar flux variations from 2014 to 2020. An interesting feature is that in 2019 the relative difference of Swarm C reaches only half the values of Swarm B, which might be related to the lower altitude of Swarm C. For MLT dependence, better agreement is also found on the dayside.

Similarly, Figure 7 shows the comparison of Ni from the FP of Swarm B and C with respect to the Ne measurements of ISR. Generally good correlations are also found between them, with correlation coefficients of 0.83 and 0.91 for the two Swarm satellites, respectively. However, different from the results of LP, the Ni from FP do not show an overall underestimation of the densities when compared to Ne from ISR. This result is consistent with the amplitude ratios of Ni between Swarm LP and FP, as shown in Figure 3. The liner regression is dominated by the points of larger values, and the Ni with higher values appear at high solar flux levels. During the higher solar flux years 2014–2016, the Ni from FP is larger than the values from the LP, therefore, it is no surprise to see that the absolute values of Ni from Swarm FP agree better with the ISR measurements. When looking at the relative differences, as shown in Figures 7b and 7e, the FP generally overestimates the plasma density, but no clear solar flux trend can be found. For the MLT dependence, it seems the FP generally overestimates the Ni on the dayside, while understates the Ni during post-midnight hours.

In the next step, we have derived the scaling factor between Ni from Swarm and Ne from the ISR. Their dependence on the solar flux index, P10.7, is shown in Figure 8, separately for the (left) LP and (right) FP measurements. The scaling factor from each conjunction is presented by a black circle, and the results have been grouped into bins according to the corresponding range of P10.7. The median values of each P10.7 bin (bin sizes of 10 sfu) are marked with red triangles. As expected, for LP, the ratios show a clear dependence on P10.7, with a steeper slope for Swarm B, while no clear dependence on P10.7 is found for the ratios with FP. The linear regression shown in Figures 8a and 8c provides direct evidence that a scaling factor exists in the Swarm LP measured Ni, which depends on the solar flux levels. The derived parameters of our linear regressions could be implemented in further updates of the Swarm LP data product.

## 5. Discussion

Due to the long-time coverage of the Swarm mission, flying in space over 8 years, the in-situ plasma densities measured by the Swarm LP become an important data source for investigating the structure and phenomena of the topside ionosphere. For a satellite mission, it is usually essential to conduct a comprehensive validation of its measurements against already existing operational instruments, to check the reliability of the data set. The Ne measured by the Swarm LP have been compared with observations from ISRs, ionosondes, and Constellation Observing System for Meteorology, Ionosphere, and Climate (COSMIC) satellites, which shows that the Swarm LP underestimated the Ne by about 21% compared to the ISR values (Lomidze et al., 2018). Though the electron density derived from Swarm LP (Baseline 04) has been changed to ion density now (Baseline 05) (Catapano et al., 2021), the comparison with ISR Ne measurements at Jicamarca still reveals an overall underestimation of the Ni data by about 25% for the three Swarm satellites. The similar underestimations between the LP derived Ne/Ni against the ISR Ne measurements suggests that the changing of the Swarm plasma density processor, by using ion current instead of electron current, does not sufficiently affect the accuracy of the derived plasma densities. This result also implies that the updated processor is consistent with pervious release.

In addition to the overall underestimation of the Swarm LP derived plasma densities, the main issue we want to address in this study is the fact that Swarm LP seems to overestimate the Ni under low solar activity conditions. Figures 6b and 6d show that the annual mean difference between Swarm Ni and ISR Ne changes from negative to positive in 2017. As the data set considered in Lomidze et al. (2018) lasts from December 2013 to June 2016, which does not cover the low solar activity years 2018 and 2019, no overestimation of Swarm LP data was found by Lomidze et al. (2018). One concern from our side is that the change of Swarm LP measured

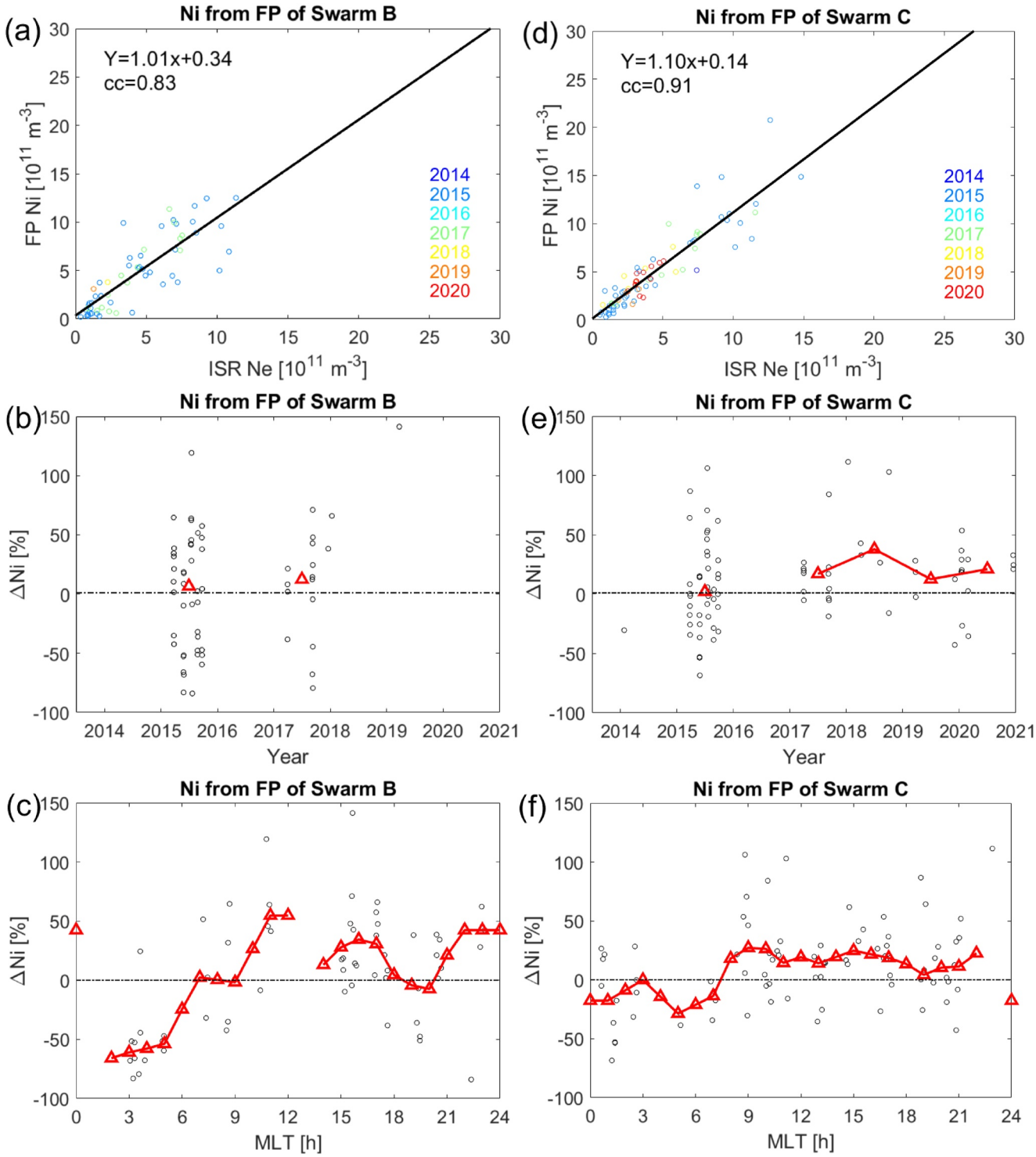


**Figure 7.** The same as Figure 6, but for the FP derived Ni and ISR Ne.

Ni from underestimation to overestimation could be due to the performance regression of the LP over the years. For example, one of the two Swarm probe's surface is made of gold-plated Titanium to reduce the aggressive chemical reactions with ionospheric Oxygen, but it is unknown how much *Au* is left on the *Ti* surface after more than 8 years in space (Catapano et al., 2021). However, as shown in our Figure 6d, the overestimation of Swarm LP Ni reduced again in 2020, which excludes the possibility of regressive performance of the LP. On the other

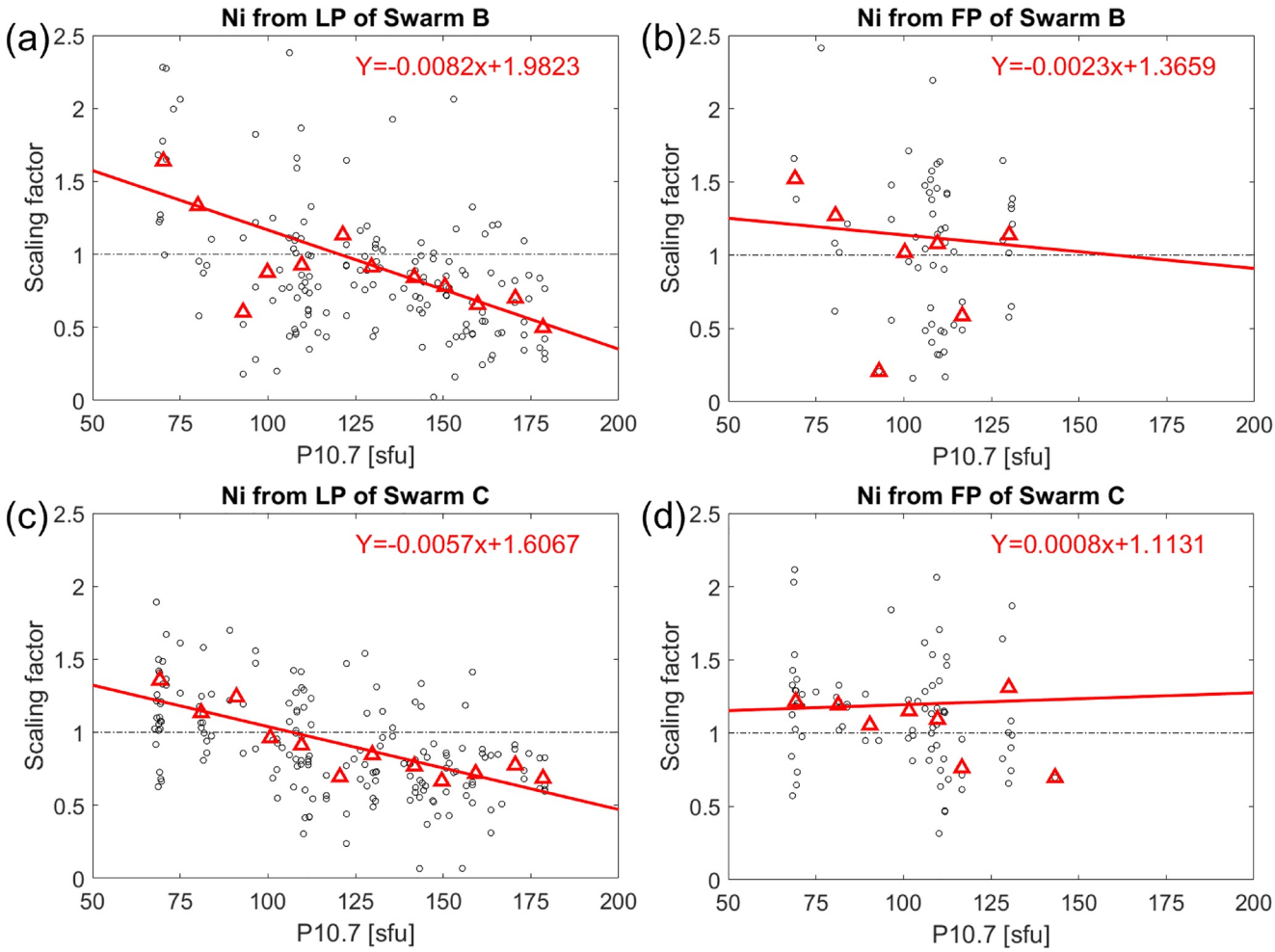


**Figure 8.** Dependence of the Swarm LP (left) and faceplate (FP) derived Ni (right) scaling factors with respect to the incoherent scatter radar Ne on the solar flux index, P10.7. Linear regression results are listed in the frames. The results from Swarm B and C are separately presented in the top and bottom frames.

hand, the variation of the ratio between Swarm LP Ni and ISR Ne shows a consistent dependence on solar flux from 2014 to 2020, thus suggesting that the solar flux plays an important role in affecting the plasma density measurements from the Swarm LP.

Additionally, the simultaneous Ni measurements from both LP and FP on board the same platform provide a good opportunity for checking the consistency and reliability of the two instruments. Our results show that there exists a systematic difference between the densities measured by the two instruments, and it changes with solar flux levels. The correlation between FP Ni and ISR Ne is slightly lower than that between LP Ni and ISR Ne, which might probably be due to fewer data points in the conjunction between FP and ISR. However, as shown in Figures 7b and 7d, the relative difference between the Swarm FP Ni and ISR Ne do not show a clear dependence over years (or solar flux level). This implies, the solar flux dependence of the systematic difference between LP and FP comes from the LP measured Ni.

When deriving the plasma densities from the LP, certain assumptions are needed for resolving the analytic I-V characteristics. In the original orbital motion limited (OML) theory the plasma is assumed to be: (a) Maxwellian distributed; (b) unmagnetized; (c) collisionless; and (d) sufficiently tenuous or hot that the Debye length is much larger than the size of the spherical or cylindrical probes (Chen, 2009; Tonks & Langmuir, 1929). The assumptions (a and c) seem to be satisfied at ionospheric F-region height under most conditions (e.g., Niyogi & Cohen, 1973). One exception is at auroral latitudes where non-thermalized energetic particles precipitate from the magnetosphere. In addition, the effects of magnetic fields on the LP measured density have also been investigated

theoretically (Rubinstein & Laframboise, 1983; Sanmartin, 1970) and experimentally (Brown et al., 1971; Ryan et al., 2019). Resendiz Lira and Marchand (2021) have performed detailed simulations for checking the possible influences of the orbital motion limited (OML) analytic approximations for the Swarm LP measured densities. One resulting concern is that the LP spheres are mounted quite close to the platform (about 99.01 mm), which could intercept or deflect the incoming particles. The result from Resendiz Lira and Marchand (2021) showed that the relative errors of the estimated electron density can reach 100% due to the platform induced electric field. In addition, when there are lighter ions (e.g., $H^+$) in the incident plasma, which are deflected more by the platform the relative error in the OML-predicted electron density can reach 50% if solely ionized oxygen ($O^+$) are assumed.

A similar concern about the influence of lighter ions causing errors in the Swarm LP derived plasma density has been raised by Catapano et al. (2021), as in the Swarm Level-1B PLASMA processor it is assumed that the plasma at Swarm height consists only of $O^+$ ions. This might be true for high solar flux years. However, as reported from the observations of Communication/Navigation Outage Forecasting System satellite, the transition height between $O^+$ and $H^+$ was reduced to about 450 km during the last solar minimum years 2008–2009 (Heelis et al., 2009). As the solar flux level during 2018–2019 stays as low as the one in 2008–2009, the transition height might also decrease to about 450 km, causing a considerable portion of $H^+$ ions at the Swarm altitude, which further challenges the Ni derivation from LP.

According to the Swarm LP processing algorithm (Buchert, 2018):

$$\mathrm{Ni}_{\mathrm{LP}} = \frac{m_i u_i}{2\pi (e r_p)^2} d_{\mathrm{ion}} \tag{1}$$

where $m_i$ is the ion mass, $u_i$ is the ion ram velocity relative to the probe, $e$ is the elementary charge, $r_p$ is the probe radius, $d_{\mathrm{ion}}$ is the ion admittance. In the current applied algorithm, a pure $O^+$ composition is assumed. Light ions (e.g., $H^+$) are expected to diffuse from the plasmasphere to the Swarm altitudes, particularly for low solar activity. Therefore, one should multiply with an effective mass $m_i$ smaller than 16 (for $O^+$), and a lower $\mathrm{Ni}_{\mathrm{LP}}$ will be obtained. Thus, a contribution of $H^+$ that is not taken into account in the processing leads to an overestimation of the derived ion density. This explains well the solar flux dependence of Ni derived from the Swarm LP, as shown in Figures 6 and 8. As Swarm B flies 50–60 km higher than Swarm C, the linear regression from Swarm B shows a steeper slope on solar flux dependence and the relative error at the altitude of Swarm B is larger.

However, the Ni derivation from FP is in a first approximation proportional to the ion charge and ion bulk drift in the normal direction (Buchert, 2017):

$$\mathrm{Ni}_{\mathrm{FP}} = \frac{I_{\mathrm{FP}}}{\mathrm{eAu}_i} \tag{2}$$

where $I_{\mathrm{FP}}$ is the faceplate current, $e$ is the elementary charge, $A$ is the faceplate area, $u_i$ is the ion velocity normal to the faceplate surface. Thus, no assumption on the plasma composition is needed for deriving $\mathrm{Ni}_{\mathrm{FP}}$. As a result, $\mathrm{Ni}_{\mathrm{FP}}$ does not show a clear solar flux dependence, though slightly larger values than those from the ISR (Figure 8). Furthermore, the much lower ratio between Swarm FP and LP derived Ni on the nightside (Figure 4) also suggests that the transition height might be lower during the night and therefore more light ions are accumulated at Swarm altitudes during the dark hours.

## 6. Summary

In this study, we performed a detailed comparison between Ni measured by the LP and FP instruments on board the Swarm satellites. Our findings can be summarized as

1. There exists a systematic difference between the Ni derived from Swarm LP and FP, and the systematic difference shows dependences on solar flux level, local time and season
2. Both the Swarm LP and FP derived Ni show generally good linear regression with Ne from the ISR at Jicamarca. However, the Ni from LP exhibit an additional dependence on the solar flux, while such a dependence cannot be seen in the FP derived Ni
3. The solar flux dependence of LP derived Ni is assumed to be related to the ion compositions change at measurement heights. A pure $O^+$ plasma is assumed in the LP processing algorithm. Light ions (e.g., $H^+$) are

expected to diffuse from the plasmasphere to the Swarm altitudes, particularly for low solar activity. With the assumption of a pure $O^+$ plasma for the Swarm data this seems to cause an overestimation of Ni from the LP, depending on the solar flux level

4. A scaling factor is defined by dividing the ISR Ne to Ni of Swarm LP, and the scaling factor shows a good linear dependence on the solar flux index, P10.7. We suggest that the derived linear regression as shown in our Figure 8 could be implemented into further updates of the Swarm LP data

$$\text{Swarm B}: \text{Ni}_{\text{LPcorr}} = -0.0082 \times V_{P10.7} + 1.9823 \quad (3)$$

$$\text{Swarm A and C}: \text{Ni}_{\text{LPcorr}} = -0.0057 \times V_{p10.7} + 1.6067 \quad (4)$$

here, the $Vp10.7$ is the value of solar flux index, P10.7. For a given solar flux level, the linear regression outlined above can be applied to the Swarm Level-1B Ni data, for correcting the solar flux influence. The LT dependence will then be a remaining issue for correction.

## Data Availability Statement

The Swarm data are provided by ESA at https://earth.esa.int/web/guest/swarm/data-access, the ISR data is available at http://cedar.openmadrigal.org/, and the solar flux indices are available at OMNIWeb database https://omniweb.gsfc.nasa.gov/.

**Acknowledgments**
This work is supported by the National Natural Science Foundation of China (42174191), the start-up program of Wuhan University (600460020), as well the Dragon five cooperation 2020–2024 (project no. 59236). Chao Xiong is supported by the Special Found of Hubei Luojia Laboratory (220100011).

## References

Appleton, E. V. (1946). Two anomalies in the ionosphere. *Nature*, *57*(3995), 691. https://doi.org/10.1038/157691a0

Astafyeva, E., Zakharenkova, I., & Pineau, Y. (2016). Occurrence of the dayside three-peak density structure intheF2and the topside ionosphere. *Journal of Geophysical Research: Space Physics*, *121*(7), 6936–6949. https://doi.org/10.1002/2016JA022641

Benson, R. F., Bauer, P., Brace, L. H., Carlson, H. C., Hagen, J., Hanson, W. B., et al. (1977). Electron and ion temperatures—A comparison of ground based incoherent scatter and AE-C measurements. *Journal of Geophysical Research*, *82*(1), 36–42. https://doi.org/10.1029/ja082i001p00036

Bilitza, D., & Xiong, C. (2020). A solar activity correction term for the IRI topside electron density model. *Advances in Space Research*, *68*(5), 2124–2137. https://doi.org/10.1016/j.asr.2020.11.012

Brace, L. H. (1998). Langmuir probe measurements in the ionosphere. *Geophysical Monograph-American Geophysical Union*, *102*, 23–36. https://doi.org/10.1029/gm102p0023

Brace, L. H., Carignan, G. R., & Findlay, J. A. (1971). Evaluation of ionospheric electron temperature measurements by cylindrical probes. *Space Research*, *11*, 1079–1105.

Brown, I. G., Compher, A. B., & Kunkel, W. B. (1971). Response of a Langmuir probe in a strong magnetic field. *The Physics of Fluids*, *14*(7), 1377–1383. https://doi.org/10.1063/1.1693617

Buchert, S. (2017). *Extended EFI LP data FP release notes*. Retrieved from https://earth.esa.int/eogateway/documents/20142/37627/SW-RN-IRF-GS-005_Extended_LP_Data_Probes.pdf

Buchert, S. (2018). *Langmuir probe level 1b algorithm*. Retrieved from https://earth.esa.int/eogateway/documents/20142/37627/swarm-level-1b-plasma-processor-algorithm.pdf/bae64759-b901-d961-4d18-0a5b317f8c12

Buchert, S., Zangerl, F., Sust, M., André, M., Eriksson, A., Wahlund, J., & Opgenoorth, H. (2015). SWARM observations of equatorial electron densities and topside GPS track losses. *Geophysical Research Letters*, *42*(7), 2088–2092. https://doi.org/10.1002/2015GL063121

Catapano, F., Buchert, S., Qamili, E., Nilsson, T., Bouffard, J., Siemes, C., et al. (2021). Swarm Langmuir Probes' data quality and future improvements. *Geoscientific Instrumentation, Methods and Data Systems*, *11*(1), 149–162. https://doi.org/10.5194/gi-2021-17

Chapkunov, S. K., Ivanova, T. N., Petrunova, M. K., & Serafimov, K. B. (1976). Measurement of electron and ion density and temperature on the INTERCOSMOS 12 satellite. *Space research XVI*, 423–425. Proceedings of the Open Meetings of Working Groups on Physical Sciences, May 29–June 7 1975.

Chen, F. F. (2009). Langmuir probes in plasma: Surprising validity of OML theory. *Plasma Sources Science and Technology*, *18*(3), 035012. https://doi.org/10.1088/0963-0252/18/3/035012

Friis-Christensen, E., Lühr, H., Knudsen, D., & Haagmans, R. (2008). Swarm—An Earth observation mission investigating Geospace. *Advances in Space Research*, *41*(1), 210–216. https://doi.org/10.1016/j.asr.2006.10.008

Hanson, W. B., Brace, L. H., Dyson, P. L., & McClure, J. P. (1969). Conflicting electron temperature measurements in the upper F region. *Journal of Geophysical Research*, *74*(1), 400–401. https://doi.org/10.1029/JA074i001p00400

Heelis, R. A., Coley, W. R., Burrell, A. G., Hairston, M. R., Earle, G. D., Perdue, M. D., et al. (2009). Behavior of the O+/H+ transition height during the extreme solar minimum of 2008. *Geophysical Research Letters*, *36*, L00C03. https://doi.org/10.1029/2009GL038652

Jin, Y., Xiong, C., Clausen, L., Spicher, A., Kotova, D., Brask, S., et al. (2020). Ionospheric plasma irregularities based on in situ measurements from the Swarm satellites. *Journal of Geophysical Research: Space Physics*, *124*(7), e2020JA028103. https://doi.org/10.1029/2020JA028103

Knudsen, D., Burchill, J., Buchert, S., Eriksson, A., Gill, R., Wahlund, J.-E., et al. (2017). Thermal ion imagers and Langmuir probes in the swarm electric field instruments. *Journal of Geophysical Research: Space Physics*, *122*(2), 2655–2673. https://doi.org/10.1002/2016JA022571

Lebreton, J. P., Stverak, S., Travnicek, P., Maksimovic, M., Klinge, D., Merikallio, S., et al. (2006). The Langmuir probe experiment processing onboard demeter: Scientific objectives, description and first results. *Planetary and Space Science*, *54*(5), 472–486. https://doi.org/10.1016/j.pss.2005.10.017

Lei, J., Syndergaard, S., Burns, A. G., Solomon, S. C., Wang, W., Zeng, Z., et al. (2007). Comparison of COSMIC ionospheric measurements with ground-based observations and model predictions: Preliminary results. *Journal of Geophysical Research*, *112*(A7), A07308. https://doi.org/10.1029/2006ja012240

Lomidze, L., Knudsen, D. J., Burchill, J., Kouznetsov, A., & Buchert, S. C. (2018). Calibration and validation of Swarm plasma densities and electron temperatures using ground-based radars and satellite radio occultation measurements. *Radio Science*, *53*(1), 15–36. https://doi.org/10.1002/2017RS006415

Lühr, H., Park, J., Gjerloev, J. W., Rauberg, J., Michaelis, I., Merayo, J. M. G., & Brauer, P. (2014). Field-aligned currents' scale analysis performed with the Swarm constellation. *Geophysical Research Letters*, *42*, 1–8. https://doi.org/10.1002/2014GL062453

McClure, J. P., Hanson, W. B., Nagy, A. F., Cicerone, R. J., Brace, L. H., Baron, M., et al. (1973). Comparisons of *Te* and *Ti* from OGO-6 and from various incoherent scatter radars. *Journal of Geophysical Research*, *78*(1), 197–205. https://doi.org/10.1029/ja078i001p00197

McNamara, L. F., Cooke, D. L., Valladares, C. E., & Reinisch, B. W. (2007). Comparison of CHAMP and digisonde plasma frequencies at Jicamarca, Peru. *Radio Science*, *42*(2), RS2005. https://doi.org/10.1029/2006RS003491

Mott-Smith, H. M., & Langmuir, I. (1926). The theory of collectors in gaseous discharges. *Physics Review*, *28*(4), 727–763. https://doi.org/10.1103/PhysRev.28.727

Niyogi, K. K., & Cohen, I. M. (1973). Continuum electrostatic probe theory with magnetic field. *The Physics of Fluids*, *16*(1), 69–74. https://doi.org/10.1063/1.1694175

Oyama, K. (2015). DC Langmuir probe for measurement of space plasma: A brief review. *Journal of Astronomy and Space Sciences*, *32*(3), 167–180. https://doi.org/10.5140/JASS.2015.32.3.167

Pedatella, N. M., Yue, X., & Schreiner, W. S. (2015). Comparison between GPS radio occultation electron densities and in situ satellite observations. *Radio Science*, *50*(6), 518–525. https://doi.org/10.1002/2015RS005677

Reigber, C., Lühr, H., & Schwintzer, P. (2002). CHAMP mission status. *Advances in Space Research*, *30*(2), 129–134. https://doi.org/10.1016/s0273-1177(02)00276-4

Resendiz Lira, P. A., & Marchand, R. (2021). Simulation inference of plasma parameters from Langmuir probe measurements. *Earth and Space Science*, *8*(3), e2020EA001344. https://doi.org/10.1029/2020EA001344

Rodríguez-Zuluaga, J., & Stolle, C. (2019). Interhemispheric field-aligned currents at the edges of equatorial plasma depletions. *Scientific Reports*, *9*(1), 1233. https://doi.org/10.1038/s41598-018-37955-z

Rother, M., Schlegel, K., Lühr, H., & Cooke, D. (2010). Validation of CHAMP electron temperature measurements by incoherent scatter radar data. *Radio Science*, *45*(6), RS6020. https://doi.org/10.1029/2010RS004445

Rubinstein, J., & Laframboise, J. (1983). Theory of axially symmetric probes in a collisionless magnetoplasma: Aligned spheroids, finite cylinders, and disks. *Physics of Fluids*, *26*(12), 3624–3627. https://doi.org/10.1063/1.864123

Ryan, P. J., Bradley, J. W., & Bowden, M. D. (2019). Comparison of Langmuir probe and laser Thomson scattering for plasma density and electron temperature measurements in hipims plasma. *Physics of Plasmas*, *26*(4), 040702. https://doi.org/10.1063/1.5094602

Sagawa, E., Immel, T. J., Frey, H. U., & Mende, S. B. (2005). Longitudinal structure of the equatorial anomaly in the nighttime ionosphere observed by IMAGE/FUV. *Journal of Geophysical Research*, *110*(A11), A11302. https://doi.org/10.1029/2004JA010848

Sanmartin, J. R. (1970). Theory of a probe in a strong magnetic field. *Physics of Fluids*, *13*(1), 103–116. https://doi.org/10.1063/1.1692776

Shen, X., Zhang, X., Yuan, S., Wang, L., Cao, J., Huang, J., et al. (2018). The state-of-the-art of the China Seismo-Electromagnetic Satellite mission. *Science China Technological Sciences*, *61*(5), 634–642. https://doi.org/10.1007/s11431-018-9242-0

Smirnov, A., Shprits, Y., Zhelavskaya, I., Lühr, H., Xiong, C., Goss, A., et al. (2021). Inter-calibration of the plasma density measurements in Earth's topside ionosphere. *Journal of Geophysical Research: Space Physics*, *126*(10), e2021JA029334. https://doi.org/10.1029/2021JA029334

Tapley, B. D., Bettadpur, S., Watkins, M., & Reigber, C. (2004). The gravity recovery and climate experiment: Mission overview and early results. *Geophysical Research Letters*, *31*(9), L09607. https://doi.org/10.1029/2004GL019920

Thébault, E., Vigneron, P., Langlais, B., & Hulot, G. (2016). A Swarm lithospheric magnetic field model to SH degree 80. *Earth Planets and Space*, *68*(1), 126. https://doi.org/10.1186/s40623-016-0510-5

Tonks, L., & Langmuir, I. (1929). A general theory of the plasma of an arc. *Physical Review*, *34*(6), 876–922. https://doi.org/10.1103/physrev.34.876

Wang, X., Cheng, W., Zhou, Z., Xu, S., Yang, D., & Cui, J. (2019). Comparison of CSES ionospheric RO data with COSMIC measurements. *Annales Geophysicae*, *37*(6), 1025–1038. https://doi.org/10.5194/angeo-37-1025-2019

Wan, X., Xiong, C., Gao, S., Huang, F., Liu, Y., Aa, E., et al. (2021). The nighttime ionospheric response and occurrence of equatorial plasma irregularities during geomagnetic storms: Case studyn. *Satellite Navigation*, *2*(1), 23. https://doi.org/10.1186/s43020-021-00055-x

Wan, X., Xiong, C., Rodriguez-Zuluaga, J., Kervalishvili, G. N., Stolle, C., & Wang, H. (2018). Climatology of the occurrence rate and amplitudes of local time distinguished equatorial plasma depletions observed by Swarm satellite. *Journal of Geophysical Research: Space Physics*, *123*(4), 3014–3026. https://doi.org/10.1002/2017JA025072

Xiong, C., Lühr, H., & Ma, S. Y. (2013). The subauroral electron density trough: Comparison between satellite observations and IRI-2007 model estimates. *Advances in Space Research*, *51*(4), 536–544. https://doi.org/10.1016/j.asr.2011.09.021

Xiong, C., Lühr, H., Ma, S., & Schlegel, K. (2015). Validation of GRACE electron densities by incoherent scatter radar data and estimation of plasma scale height in the topside ionosphere. *Advances in Space Research*, *55*(8), 2048–2057. https://doi.org/10.1016/j.asr.2014.07.022

Xiong, C., Stolle, C., Lühr, H., Park, J., Fejer, B. G., & Kervalishvili, G. N. (2016). Scale analysis of the equatorial plasma irregularities derived from Swarm constellation. *Earth Planets and Space*, *68*(1), 121. https://doi.org/10.1186/s40623-016-0502-5

Xiong, C., Zhou, Y.-L., Lühr, H., & Ma, S.-Y. (2016). Diurnal evolution of the F region electron density local time gradient at low and middle latitudes resolved by the Swarm constellation. *Journal of Geophysical Research: Space Physics*, *121*(9), 9075–9089. https://doi.org/10.1002/2016JA023034

Yan, R., Zhima, Z., Xiong, C., Shen, X., Huang, J., Guan, Y., et al. (2020). Comparison of electron density and temperature from the CSES satellite with other space-borne and ground-based observations. *Journal of Geophysical Research: Space Physics*, *125*(10), e2019JA027747. https://doi.org/10.1029/2019JA027747

Zhou, Y.-L., Lühr, H., Xiong, C., & Pfaff, R. F. (2016). Ionospheric storm effects and equatorial plasma irregularities during the 17–18 March 2015 event. *Journal of Geophysical Research: Space Physics*, *121*(9), 9146–9163. https://doi.org/10.1002/2016JA023122